Journal of Materials Chemistry C

ROYAL SOCIETY OF CHEMISTRY

COMMUNICATION

View Article Online
View Journal | View Issue

Cite this: J. Mater. Chem. C, 2025, 13, 23371

Received 22nd August 2025,
Accepted 14th November 2025

DOI: 10.1039/d5tc03167b

rsc.li/materials-c

Redox-switchable gelation of unmodified cellulose nanocrystals

Yota Neagari, †[a] Zongzhe Li [a] and Mark J. MacLachlan *[abcd]

We demonstrate a redox-switchable gelation system for unmodified cellulose nanocrystals (CNCs) driven by the oxidation of ferrocene (Fc). Upon oxidation of Fc to ferrocenium (Fc^+), achieved either chemically or electrochemically, the increased ionic strength screens electrostatic repulsion between negatively charged CNC rods, thereby inducing physical gelation. The gel strength can be reversibly modulated: oxidation produces a strong gel, and subsequent reduction weakens it. Multiple redox cycles enable repeated switching, although complete recovery of the initial fluidity is not obtained. Rheological, spectroscopic, and electrochemical analyses confirm that the gelation arises from Fc^+-mediated electrostatic screening without any chemical modification of CNCs. This simple, additive-driven strategy provides a sustainable platform for electro-responsive soft materials from renewable nanocrystals, with potential applications in drug delivery, microfluidic valves, and electro-assisted 3D printing.

Introduction

Stimuli-responsive gels are soft materials that show changes in properties (*e.g.* viscosity, volume, and sol–gel state) in response to external stimuli such as temperature, pH, light, and redox inputs.[1–4] These "smart" gels have attracted significant attention for applications in drug delivery, sensing, soft actuators, and self-healing materials.[5–7] Among various stimuli, redox control is particularly appealing because it enables on-demand modulation of gel properties through the addition of redox agents or the application of an electric potential.[8–14] This approach offers spatially and temporally precise control over gelation or dissolution, making it highly promising for technologies such as electro-assisted 3D printing and microfluidic systems.[15–18]

Thermo-responsive gels undergo sol–gel transitions driven by temperature-induced dehydration of polymer chains,[1,2,19] while photo-responsive systems rely on photo-isomerization or photo-cleavage to alter cross-linking density.[1,2,20] pH-responsive gels regulate electrostatic interactions through protonation/deprotonation equilibria.[1,2,21] Although these mechanisms enable rapid gelation, they often require specific polymer architectures, covalent incorporation of functional groups, or defined chemical environments. In contrast, redox reactions offer a versatile approach that can be triggered chemically or electrochemically to reversibly modulate gel structure and properties.

Redox-responsive gels commonly incorporate redox-active components such as ferrocene or iron ions within polymer networks to induce reversible cross-linking or coordination.[8–14] These systems exhibit tunable viscoelasticity and ionic conductivity *via* electron-transfer-induced structural reorganization.[22,23] However, most reported examples rely on covalent functionalization or supramolecular host–guest interactions, necessitating tailored molecular designs that limit material scope and scalability.

Ferrocene (Fc) is one of the most widely used redox-active units for imparting redox-responsiveness to gels due to its reversible Fc/ferrocenium (Fc^+) redox couple.[9,24] Previous approaches have primarily relied on covalent incorporation of Fc units into polymer backbones or small molecules, or on constructing redox-responsive supramolecular gels through host–guest interactions with macrocycles such as β-cyclodextrins and pillar[*n*]arenes, which exhibit distinct binding affinities toward Fc and Fc^+.[15,25,26] While these systems can achieve tunable mechanical properties, they often require complex synthesis, covalent modification, or intricate molecular designs, limiting their scalability and material diversity.

Cellulose nanocrystals (CNCs) are rod-like, renewable, and biocompatible nanomaterials obtained from natural sources such as wood pulp, cotton, and other biomass *via* acid

[a] Department of Chemistry, University of British Columbia, 2036 Main Mall, Vancouver, BC V6T 1Z1, Canada. E-mail: mmaclach@chem.ubc.ca
[b] Stewart Blusson Quantum Matter Institute, University of British Columbia, 2355 East Mall, Vancouver, BC, V6T 1Z4, Canada
[c] WPI Nano Life Science Institute, Kanazawa University, Kanazawa, 920-1192, Japan
[d] Bioproducts Institute, University of British Columbia, 2360 East Mall, Vancouver, BC, V6T 1Z3, Canada
† Y. N. is also affiliated with Mitsubishi Materials Corporation, 3-2-3, Marunouchi, Chiyoda-ku, Tokyo, 100-8117, Japan.

hydrolysis of cellulose.[27,28] CNC surfaces prepared by sulfuric acid hydrolysis bear sulfate half-ester groups, imparting negative charges and enabling stable colloidal dispersions through electrostatic repulsion. CNC suspensions can undergo physical gelation *via* several pathways, including surface charge neutralization, electrostatic screening, desulfation, and freeze–thawing.[29–31] Among these, pH-induced charge neutralization and electrolyte-driven screening are commonly employed to suppress repulsion and enhance interparticle attraction among CNCs.[32–36] Despite extensive research on CNC-based physical gels, most examples exhibit irreversible gelation, and only a few cases have demonstrated reversible property changes in response to stimuli such as pH or temperature.[32,37–42] Although Fc derivatives have been combined with CNCs in prior studies, their use to achieve redox-responsive CNC gelation has not been reported.[43,44]

In our previous work, we developed a CO_2-responsive gelation system for CNC suspensions triggered by imidazole protonation.[45] CO_2 lowers the pH through carbonic acid formation, converting imidazole into imidazolium cations, which increases ionic strength and screens electrostatic repulsion, leading to gelation. Removing CO_2 by purging the gel with N_2 restores the pH and reverses gelation. Inspired by this mechanism, we hypothesized that a redox-active additive such as Fc, which generates cationic Fc^+ species upon oxidation, could similarly modulate ionic strength and enable reversible control of CNC gel strength without chemical modification of the CNCs. Preliminary observations of Fc-induced gelation of CNC suspensions were reported in a PhD thesis,[46] but reversible redox cycling, electrochemical control, and mechanistic elucidation were not addressed.

Here, we demonstrate a redox-responsive gelation system for unmodified CNC suspensions in which oxidation of Fc to Fc^+ increases ionic strength, screens the surface charges of CNCs, and induces aggregation and gel formation (Fig. 1(a) and (b)). Gel strength can be reversibly modulated by chemical oxidation and reduction, and electrochemical control of gelation is also demonstrated. Rheological measurements confirmed the modulation of gel strength through oxidation–reduction–re-oxidation cycles, while complementary spectroscopic, ζ potential, and scanning electron microscopy analyses were conducted to elucidate the underlying mechanism. The system responds reproducibly to redox cycling, representing a simple, sustainable, and additive-driven strategy for developing redox-responsive soft materials from renewable nanocrystals without covalent modification.

Materials and methods

Materials

All chemicals were obtained from Sigma-Aldrich, Tokyo Chemical Industry (TCI), and Fisher Scientific, and used without further purification. Ferrocene (Fc) was purified by sublimation before use. An aqueous CNC suspension was provided by FPInnovations in acidic form (CNC-H^+, 5.1 wt%, pH = 2.2, and conductivity = 1.9 mS cm^{-1}). The average length of CNC spindles was determined by transmission electron microscopy (TEM) to be 280 ± 90 nm (Fig. S1, SI). In addition to TEM, the particle size was evaluated by dynamic light scattering (DLS), showing an average hydrodynamic diameter of 274 ± 18 nm (PDI = 0.25). Moreover, the presence of sulfate half-ester groups on the CNC surfaces was evaluated using zeta potential, yielding a value of −57.6 ± 0.8 mV. However, the sulfur content of freeze-dried CNC-H^+ was below the detection limit (<0.5 wt%) of the elemental analysis (EA) performed with a Thermo Flash 2000 Elemental Analyzer. Indium tin oxide (ITO) glass

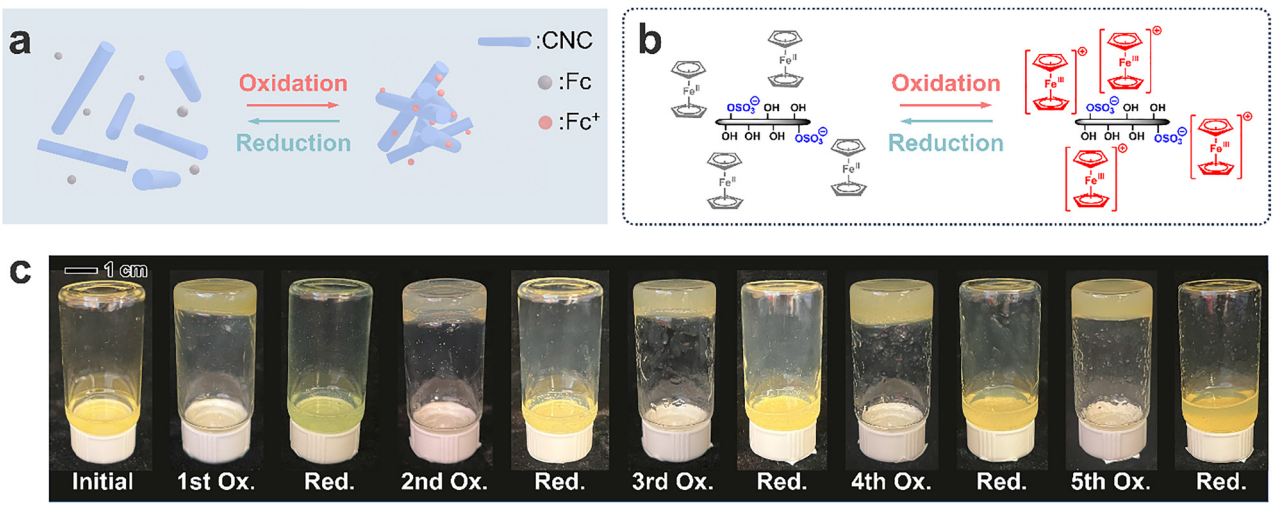

Fig. 1 Redox-responsive gelation of CNC/Fc systems. (a) Schematic illustration of reversible transitions between dispersed and aggregated CNC states induced by redox switching between Fc and Fc^+. (b) Proposed mechanism of electrostatic interactions between sulfate half-ester groups on CNCs and Fc or Fc^+ species. (c) Photographs showing visual changes in gel strength of a CNC/Fc suspension (3 wt% CNC, H_2O–DMSO (1 : 1), Fc 3.2 mM) over five redox cycles. Each cycle involved oxidation with aqueous H_2O_2 solution (9.8 M, 20 μL, 20 equiv. for the first cycle and 50 equiv. for subsequent cycles) at 60 °C for 30 min, followed by reduction with aqueous ascorbic acid solution (1.5 M, 0.3 mL, 50 equiv.) at room temperature for 5 min.

(thickness: 1.10 ± 0.05 mm; resistance per sq: 10–15 Ω; transmittance: ≥85%) was purchased from Adafruit.

Preparation of CNC suspensions

An aqueous CNC suspension (CNC-H^+, 5.1 wt%, pH = 2.2, and conductivity = 1.9 mS cm^{-1}) was diluted with deionized water to obtain a 3.0 wt% aqueous CNC suspension. To prepare a CNC suspension in dimethyl sulfoxide (DMSO), water was removed from the 5.1 wt% aqueous CNC suspension using a rotary evaporator, while gradually adding DMSO. The resulting CNC suspension was adjusted to a concentration of 3.0 wt% in DMSO. A mixed CNC suspension in 1 : 1 (v/v) H_2O–DMSO was prepared by combining equal volumes of the 3.0 wt% aqueous CNC and the 3.0 wt% CNC-in-DMSO suspensions, followed by sonication for 2 min.

Redox-controlled CNC/Fc systems

A 0.1 M Fc solution in DMSO (0.1 mL, 0.01 mmol) was added to a CNC suspension (3.0 wt%, 3.0 mL) in 1 : 1 (v/v) H_2O–DMSO in a 20 mL vial. Oxidation was induced by adding aqueous hydrogen peroxide solution (H_2O_2) (30 wt%, 20 μL, 0.2 mmol) and heating the sample at 60 °C for 30 min without agitation, producing a gel. Reduction was carried out by adding aqueous ascorbic acid solution (1.5 M, 0.3 mL, 0.5 mmol) and gently mixing, resulting in a weak gel. Re-oxidation was carried out by adding aqueous H_2O_2 solution (30 wt%, 50 μL, 0.5 mmol) and heating under the same conditions to restore the strong gel.

Electro-induced gelation of CNC/Fc systems

A 0.1 M Fc solution in DMSO (0.1 mL, 0.01 mmol) and a 1.0 M aqueous NaCl solution (30 μL, 0.03 mmol) were added to a CNC suspension (3.0 wt%, 3.0 mL) in 1 : 1 (v/v) H_2O–DMSO in a 20 mL vial. An ITO glass working electrode (submerged area: 1.0 × 1.0 cm^2), Pt mesh counter electrode, and Ag/AgCl reference electrode were immersed in the mixture. Electrochemical gelation was performed using a bipotentiostat (model AFCBP1, Pine Instrument Company) by applying +1.0 V for 1 h, resulting in gel formation.

Results and discussion

Optimization of redox-responsive gelation conditions

To optimize redox-responsive gelation, several key factors influencing CNC/Fc suspensions were investigated using the inversion test to evaluate gel strength (Table 1). Gelation occurred only when hydrogen peroxide (H_2O_2) was added to a 3 wt% CNC suspension in DMSO containing Fc (Table 1, entries 1 *vs.* 2). Under these conditions, a strong gel formed and remained stable upon vial inversion for at least 30 minutes. In a 1 : 1 (v/v) H_2O–DMSO mixture, oxidation produced a strong gel, chemical reduction weakened it, and re-oxidation restored its strength (Table 1, entry 3 and Video S1). This reversible behavior is only observed in the H_2O–DMSO system and not in neat DMSO (Table 1, entries 2 *vs.* 3). This difference is attributed to the dielectric permittivity of the solvent.[47] DMSO has a lower dielectric constant than the H_2O–DMSO mixture, which shortens the Debye length and maintains strong electrostatic screening between CNCs even after Fc^+ is reduced back to Fc.[48] As a result, gel strength remains high in DMSO. In contrast, the higher dielectric environment in the mixed solvent allows the electrostatic repulsion to be restored upon reduction, leading to a decrease in gel strength, while re-oxidation again induces gelation. This reversible switching was maintained for at least five cycles despite progressive dilution caused by repeated addition of aqueous oxidant and reductant solutions, and no visible phase separation was observed during inversion tests (Fig. 1(c)). The Fc content in the CNC suspension (3 wt% CNC in H_2O–DMSO (1 : 1)) was varied from 0.3 to 6.3 mM. No gelation was observed at 0.3 mM after oxidation, and only weak gelation occurred at 1.6 mM (Table 1, entry 4 and Table S1, entry 6). In contrast, concentrations of 3.2–6.3 mM enabled strong and reversible gel formation, although a turbid suspension was observed at 6.3 mM due to the limited solubility of Fc (Table S1, entry 7). For aqueous systems, Fc was solubilized *via* hydroxypropyl-β-cyclodextrin (HP-β-CD) inclusion complexes,[49,50] enabling similar redox behavior without the use of DMSO (Table 1, entry 5). Owing to the simplicity of the additive system, the H_2O–DMSO mixed-solvent CNC/Fc gel was adopted as the primary model in this study. At CNC concentrations of 2 wt% or lower, oxidation produced only weak gels or no gelation (Table S1, entries 8 and 9). At least 10 equiv. of H_2O_2 were required for gelation and, without heating, gel formation at room temperature required approximately 18 h (Table S1, entries 10–12). Glutathione could replace ascorbic acid as a reductant (Table S1, entry 13). In contrast, $FeCl_3$,[51] NaOCl, or $Na_2S_2O_4$ induced irreversible gelation even in the absence of Fc (Table S1, entries 14 and 15; Fig. S2, SI) likely due to their direct enhancement of the ionic strength of the system. HP-β-CD itself had little effect

Table 1 Redox-responsive behavior of CNC/Fc suspensions under select conditions. Gel states upon oxidation (Ox.), reduction (Red.), and re-oxidation (Re-Ox.) were evaluated by inspection[a]

Entry	Solv.	Fc/mM	Additive/mM	Ox.	Red.	Re-Ox.
1	DMSO	—	—	Sol	Sol	—
2	DMSO	3.2	—	Strong gel	Strong gel	—
3	**H_2O–DMSO (1 : 1)**	**3.2**	—	**Strong gel**	**Weak gel**	**Strong gel**
4	H_2O–DMSO (1 : 1)	1.6	—	Weak gel	Weak gel	—
5	H_2O	3.2	HP-β-CD/10	Strong gel	Weak gel	Strong gel

[a] CNC concentration = 3 wt%. Sol: non-gelled liquid; strong gel: self-standing gel with no flow upon vial inversion for at least 30 min; weak gel: soft gel flowing upon mild shaking. Oxidation: H_2O_2 aq. (9.8 M, 20 equiv.), 60 °C, 30 min. Reduction: ascorbic acid aq. (1.5 M, 50 equiv.), RT, 5 min. Re-oxidation: H_2O_2 aq. (9.8 M, 50 equiv.), 60 °C, 30 min.

on gelation; NaCl up to 10 mM was inactive, while 20 mM NaCl or 10 mM KCl produced weak gels (Table S1, entries 16 and 17). Methyl-β-cyclodextrin (Me-β-CD) could also replace HP-β-CD (Table S1, entry 18), with no obvious difference in the strength of resulting gels. Without cyclodextrins, Fc was insoluble in water; however, oxidation of its suspension still induced gelation, although strength recovery upon reduction was not observed (Table S1, entry 19). Finally, replacing Fc with ferrocenecarboxylic acid yielded similar redox responsiveness (Table S1, entry 20), suggesting the potential to tailor solubility and functionality by using ferrocene derivatives, as well as the versatility of our strategy.

Properties of redox-responsive CNC/Fc gels

The redox-responsive gelation behavior was examined under optimized conditions (3 wt% CNC, 3.2 mM Fc, H_2O–DMSO (1 : 1, v/v)). Rheological measurements were performed using an oscillatory rheometer with a parallel plate geometry (Fig. 2(a) and (b)). Dynamic frequency sweeps (0.1–100 rad s^{-1}) showed that in the oxidized state, the storage modulus (G') is significantly higher than the loss modulus (G'') throughout the entire tested frequency range, with the complex modulus (G^*) reaching $\sim$1.6–2.2 $\times$ 10^3 Pa, indicative of a strong gel. Upon reduction, both G' and G^* dropped markedly ($\sim$2.5–3.1 $\times$ 10^2 Pa), reflecting substantial network weakening. Re-oxidation restored G^* to $\sim$ 1.5–2.0 $\times$ 10^3 Pa, close to the initial oxidized state.

These mechanical trends correlate well with microstructural observations by scanning electron microscopy (SEM) (Fig. 2(c) and Fig. S3, SI). Aerogels were prepared from oxidized and reduced CNC/Fc gels *via* ethanol solvent exchange followed by supercritical CO_2 drying. The oxidized-gel-derived aerogel exhibited a dense, homogeneous, and highly interconnected CNC network, whereas the reduced-gel-derived aerogel showed a looser structure with larger voids and greater heterogeneity. These morphological differences align with the gel-softening behavior, supporting the notion that redox cycling induces reversible rearrangements within the CNC/Fc network.

Polarized optical microscopy (POM) images of CNC/Fc gels in the initial, oxidized, and reduced states (Fig. S4, SI) showed no birefringence, indicating the absence of long-range ordered domains. In the initial state, crystalline Fc precipitates were evident; however, they disappeared upon oxidation and did not reappear after reduction. This suggests an irreversible microscopic redistribution of Fc, which may contribute to the incomplete recovery of the original fluidity after the redox cycle.

Electro-induced gelation of CNC/Fc suspensions

Having established that chemical redox reactions can reversibly tune the strength of CNC/Fc gels, we next explored electrochemical control. Cyclic voltammetry (CV) of the CNC/Fc suspension in the presence of NaCl (10 mM) to enhance conductivity revealed a quasi-reversible one-electron redox couple characteristic of the Fc/Fc^+ pair, with an anodic peak at approximately +0.46 V and a cathodic peak at +0.17 V *vs.* Ag/AgCl at a scan rate of 50 mV s^{-1} ($\Delta E_p \approx 290$ mV) (Fig. 3(a)). The anodic peak current ($i_{p,a}$) corresponded to Fc oxidation, while the cathodic peak current ($i_{p,c}$) reflected the reverse reduction. Peak currents increased linearly with the square root of the scan rate (Fig. S5, SI), indicating a diffusion-controlled process. A solution of Fc only in 1 : 1 H_2O–DMSO displayed a similar voltammogram, whereas a suspension of only CNCs in the same solvent mixture showed no detectable redox peaks (Fig. S6, SI).

Applying a constant potential of +1.0 V *vs.* Ag/AgCl to the CNC/Fc suspension for 1 h induced gelation, converting it from a free-flowing liquid to a self-supporting gel (Fig. 3(b)). Similar results were obtained when the suspension was confined between two ITO glass plates with a 1.0 $\times$ 1.0 $\times$ 0.2 cm^3 spacer, one plate serving as the working electrode (Fig. 3(c) and Fig. S7, SI). Without an applied potential, the suspension remained fluid and readily flowed under gravity. To demonstrate spatial control, the working electrode was partially covered with a PET stencil patterned with the letters "UBC" (Fig. 3(d) and Fig. S8, SI). After 1 h at +1.0 V *vs.* Ag wire, gelation of the CNC/Fc

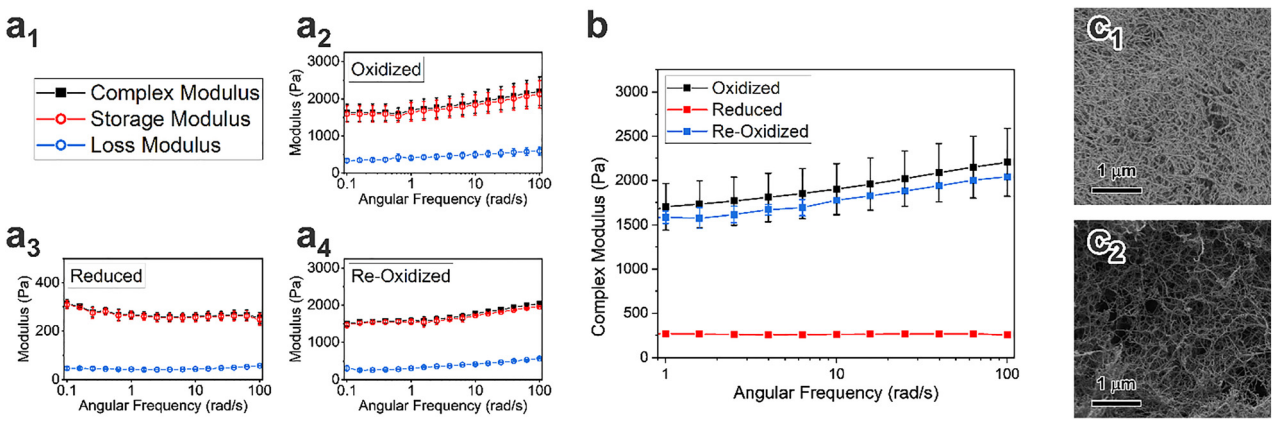

Fig. 2 (a) Frequency dependence of the complex modulus (G^*, black), storage modulus (G', red), and loss modulus (G'', blue) of CNC/Fc gels (3.0 wt% CNC, 3.2 mM Fc, H_2O–DMSO (1 : 1)); (a_1) legend, (a_2) oxidized, (a_3) reduced, and (a_4) re-oxidized states. Error bars represent the standard deviations from triplicate measurements for samples under each state. (b) Summary plot compiling the complex moduli (G^*) from (a_2)–(a_4), directly comparing oxidized (black), reduced (red), and re-oxidized (blue) states. Data shown are limited to the frequency range of 1–100 rad s^{-1} for clarity. (c) SEM images of the cross sections of aerogels prepared from oxidized (c_1) and reduced (c_2) CNC/Fc gels.

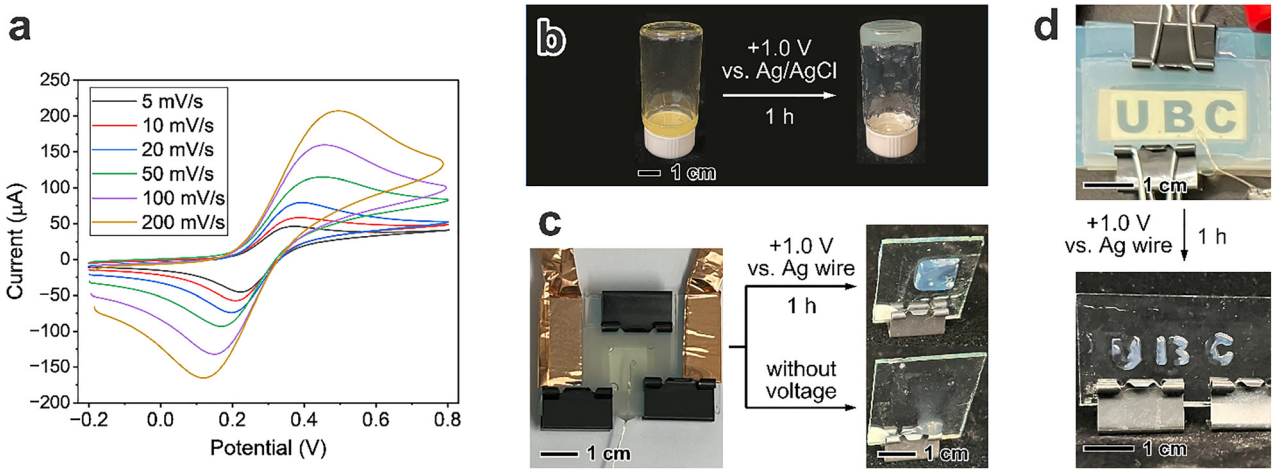

Fig. 3 (a) Cyclic voltammograms of the CNC/Fc suspension (3 wt% CNC, H_2O–DMSO (1 : 1), 3.2 mM Fc, 10 mM NaCl) at various scan rates, measured using a three-electrode system with ITO glass (1.0 × 1.0 cm^2) as the working electrode, Pt mesh as the counter electrode, and Ag/AgCl as the reference electrode. (b) Photographs of the CNC/Fc suspension before and after applying +1.0 V *vs.* Ag/AgCl for 1 h, showing the change from an initial fluid state to a gelled state. (c) Photographs of the device consisting of the CNC/Fc suspension sealed between two ITO glass plates with a 1.0 × 1.0 × 0.2 cm^3 spacer, before, after and without voltage application at +1.0 V *vs.* Ag wire for 1 h. (d) Patterned gelation of the CNC/Fc suspension on an ITO substrate using a stencil mask ("UBC" pattern) under +1.0 V *vs.* Ag wire for 1 h, demonstrating spatially controlled gel formation. In the top photograph, the "UBC" printed paper placed beneath the device serves only as a visual background for photographic clarity and is not part of the device.

suspension occurred selectively in the exposed regions, reproducing the stencil pattern with high fidelity. Although slight discontinuities were observed in the visible pattern due to removal of the non-gelled CNC/Fc suspension during visualization and inherent variations in stencil features and gel thickness, the selective gelation confined to the electrode-exposed regions demonstrates the proof-of-concept of spatially controlled electrochemical gelation.

Whereas chemical reduction softened the gels and enabled reversible modulation of gel strength, the application of negative potentials (*e.g.*, −1.0 V, 1 h) did not reproduce this weakening effect. This asymmetry likely stems from differences in reduction pathways. Ascorbic acid diffuses throughout the gel and uniformly reduces Fc^+, disrupting ionic crosslinks and softening the entire network. In contrast, electrochemical reduction is confined to regions near the electrode surface and may be limited by slow Fc^+ diffusion and strong ion-pairing with anionic CNC surfaces, thereby preventing full reduction of Fc^+ within the bulk gel.[52] As a result, the overall gel strength remains largely unchanged. Nevertheless, the demonstrated ability to trigger and spatially control gelation electrochemically highlights the versatility of this system and suggests opportunities for applications such as electrically driven 3D printing and spatially controlled fabrication.

Mechanistic insights into redox-induced gelation

To elucidate the mechanism of redox-induced gelation in the CNC/Fc suspension, spectroscopic analyses (UV-vis, ^1H NMR, FT-IR) were performed over oxidation–reduction cycles. UV-vis spectra revealed the appearance of a broad absorption band at ~620 nm upon oxidation with H_2O_2, corresponding to the ligand-to-metal charge transfer transition of the Fc^+ cation, which disappeared after reduction with ascorbic acid (Fig. S9, SI). Electrochemical oxidation at +1.0 V *vs.* Ag wire produced a similar absorption band at ~620 nm corresponding to the Fc^+ cation (Fig. S10, SI). The absorption band obtained after chemical oxidation appeared broader than that produced by electrochemical oxidation. This broadening may result from side reactions of Fc with H_2O_2,[53] and could contribute to the difference in gel responsiveness between chemical and electrochemical oxidation. In the ^1H NMR spectrum, the cyclopentadienyl proton signal of Fc at $\delta \approx 4.1$ ppm disappeared upon oxidation, indicative of conversion to the paramagnetic Fc^+ species; reduction restored the original Fc signal (Fig. S11, SI). FT-IR spectra showed no discernible changes, indicating that CNCs themselves were unaffected by the redox treatments (Fig. S12, SI).

The ζ potential of the CNC/Fc suspension was initially −22 mV (Fig. 4(a)). Oxidation increased it to −15 mV (less negative), whereas subsequent reduction restored it to −21 mV. This reversible trend was reproducible over at least three cycles. In contrast, CNC suspensions without Fc showed no significant change (−21 to −20 mV) when exposed to oxidizing or reducing agents (Fig. 4(b)). Addition of ferrocenium hexafluorophosphate ($FcPF_6$) to a control suspension of 3 wt% CNCs produced similar effects (Fig. 4(c) and Fig. S13, SI): gelation occurred, the ζ potential increased to −16 mV, and reduction decreased it back to −23 mV. Conductivity increased markedly upon oxidation in CNC/Fc suspensions but not in a CNC suspension alone, while pH changes were attributed solely to the acidity of ascorbic acid (Fig. S14 and S15, SI).

Taken together, these results indicate that redox-induced gelation is not driven by chemical changes of CNCs or by pH variation, but by ionic effects of Fc^+ (Fig. 1(a) and (b)). Oxidation generates cationic Fc^+, which increases conductivity and screens the negativity charged sulfate half-ester groups on CNC surfaces, reducing electrostatic repulsion and enabling

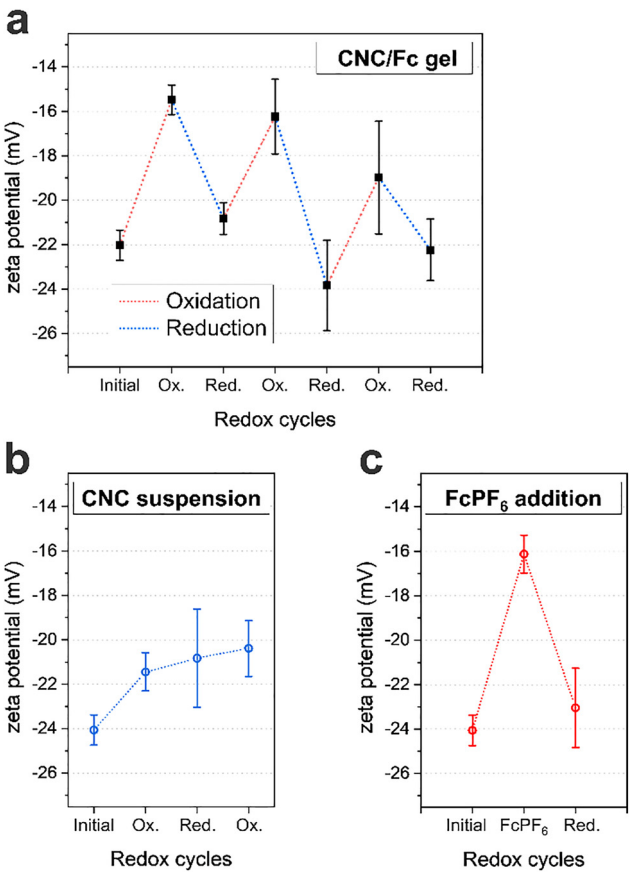

Fig. 4 ζ-potential measurements of CNC suspensions under different redox conditions. (a) CNC/Fc gels (3.0 wt% CNC, 3.2 mM Fc, H_2O–DMSO (1 : 1)) over three redox cycles. Each cycle involved oxidation with aqueous H_2O_2 solution (9.8 M, 20 μL, 20 equiv. for the first cycle and 50 equiv. thereafter) at 60 °C for 30 min, followed by reduction with aqueous ascorbic acid solution (1.5 M, 0.3 mL, 50 equiv.) at room temperature for 5 min. (b) CNC suspension (3.0 wt% CNC, H_2O–DMSO (1 : 1)) subjected to oxidation, reduction, and re-oxidation under the same conditions. (c) CNC suspension (3.0 wt% CNC, H_2O–DMSO (1 : 1)) after addition of $FcPF_6$ (3.2 mM), heating at 60 °C for 30 min, and subsequent reduction with ascorbic acid. Samples (25 mg) were diluted with Milli-Q water (10 mL) prior to measurement. Error bars represent standard deviations from replicate measurements.

network formation. Reduction restores neutral Fc and thus partially recovers electrostatic stabilization, leading to partial gel dissolution. The similar responses observed upon $FcPF_6$ addition further support this electrostatic screening mechanism.

Although gelation proceeds on a timescale of several minutes under chemical redox conditions, this kinetic behavior is consistent with diffusion-controlled ionic screening and gradual network assembly of CNC nanoparticles, rather than rapid chain conformational changes typical of polymer-based stimuli-responsive gels. Despite this slower response, this additive-based approach offers advantages in molecular simplicity and the gelation rate may be further enhanced by optimizing redox efficiency or employing more soluble or structurally optimized Fc derivatives, potentially enabling its use in future applications such as 3D printing, drug delivery, or microfluidic control.

Conclusions

We have developed a simple, additive-driven strategy to achieve redox-responsive gelation of unmodified CNC suspensions by Fc/Fc^+ cycling. Oxidation of Fc to Fc^+ increases ionic strength and screens CNC surface charges, inducing aggregation and gel formation, while subsequent chemical reduction partially restores fluidity. This mechanism enables reversible tuning of gel strength without chemical modification of CNCs, as confirmed by rheology, microscopy, and spectroscopic analyses. The ability to trigger and spatially control gelation electrochemically further expands the versatility of this system, offering a sustainable platform for developing electro-responsive soft materials with potential applications in drug delivery, microfluidic control, and electro-assisted 3D printing.

Author contributions

Y. N. designed the experiments, prepared samples, conducted the majority of measurements and analysis, and wrote the original draft of the manuscript. Z. L. performed rheological measurements, prepared aerogels, conducted SEM and TEM analyses, and assisted with ζ potential measurements. M. J. M. supervised the project, provided valuable feedback, acquired funding, contributed resources, and reviewed and revised the manuscript.

Conflicts of interest

There are no conflicts to declare.

Data availability

All experimental procedures, characterisation data, supporting spectra, electron micrographs, and other data can be found in the article or in the supplementary information (SI). Supplementary information: a supporting video (Video S1) for this work is available, showing the redox-responsive behavior of CNC/Fc suspensions. See DOI: https://doi.org/10.1039/d5tc03167b.

Acknowledgements

This work was supported by the Natural Sciences and Engineering Research Council (NSERC) of Canada (Discovery Grant) and Mitsubishi Materials Corporation. MJM thanks the Canada Research Chairs Program for support and acknowledges the Canada Foundation for Innovation (CFI) and British Columbia Knowledge Development Fund (BCKDF) for infrastructure grants (JELF 34098, 38963). ZL thanks UBC for a 4YF Fellowship. We thank Miguel Soto (UBC, now at University of Saskatchewan) for useful discussions and valuable advice on methodology development, Wadood Hamad (formerly at FPInnovations) for providing the CNCs, UBC Bioimaging Facility (Derrick Horne, RRID: SCR_021304) for SEM, and the UBC Chemistry Shared Instrument Facility (Benjamin Herring) for FTIR, and the Mass Spectrometry and Microanalytical

Laboratory at UBC for conducting elemental analysis measurements. We also acknowledge Lev Lewis for preliminary investigations into redox-responsive CNC/Fc systems described in his PhD thesis.

References

1 M. C. Koetting, J. T. Peters, S. D. Steichen and N. A. Peppas, *Mater. Sci. Eng. R Rep.*, 2015, **93**, 1–49.
2 P. Sikdar, Md. M. Uddin, T. M. Dip, S. Islam, Md. S. Hoque, A. K. Dhar and S. Wu, *Mater. Adv.*, 2021, **2**, 4532–4573.
3 S. Correa, A. K. Grosskopf, H. Lopez Hernandez, D. Chan, A. C. Yu, L. M. Stapleton and E. A. Appel, *Chem. Rev.*, 2021, **121**, 11385–11457.
4 Md. M. H. Rumon, A. A. Akib, F. Sultana, Md Moniruzzaman, M. S. Niloy, M. S. Shakil and C. K. Roy, *Polymers*, 2022, **14**, 4539.
5 Y. Zhang and B. M. Wu, *Gels*, 2023, **9**, 838.
6 M. Neumann, G. Di Marco, D. Iudin, M. Viola, C. F. Van Nostrum, B. G. P. Van Ravensteijn and T. Vermonden, *Macromolecules*, 2023, **56**, 8377–8392.
7 S. Amirthalingam, A. K. Rajendran, Y. G. Moon and N. S. Hwang, *Mater. Horiz.*, 2023, **10**, 3325–3350.
8 X. Sui, X. Feng, M. A. Hempenius and G. J. Vancso, *J. Mater. Chem. B*, 2013, **1**, 1658–1672.
9 X. Liu, L. Zhao, F. Liu, D. Astruc and H. Gu, *Coord. Chem. Rev.*, 2020, **419**, 213406.
10 X. Hou, Y. Li, Y. Pan, Y. Jin and H. Xiao, *Chem. Commun.*, 2018, **54**, 13714–13717.
11 O. Mergel, S. Schneider, R. Tiwari, P. T. Kühn, D. Keskin, M. C. A. Stuart, S. Schöttner, M. De Kanter, M. Noyong, T. Caumanns, J. Mayer, C. Janzen, U. Simon, M. Gallei, D. Wöll, P. Van Rijn and F. A. Plamper, *Chem. Sci.*, 2019, **10**, 1844–1856.
12 Z. Gao, B. Golland, G. Tronci and P. D. Thornton, *J. Mater. Chem. B*, 2019, **7**, 7494–7501.
13 T. Ikeda, *ACS Appl. Polym. Mater.*, 2023, **5**, 839–845.
14 B. Arsuffi, G. Siqueira, G. Nyström, S. Titotto, T. Magrini and C. Daraio, *Adv. Funct. Mater.*, 2024, **34**, 2409864.
15 M. Nakahata, Y. Takashima, H. Yamaguchi and A. Harada, *Nat. Commun.*, 2011, **2**, 511.
16 M. Fadeev, G. Davidson-Rozenfeld, Y. Biniuri, R. Yakobi, R. Cazelles, M. A. Aleman-Garcia and I. Willner, *Polym. Chem.*, 2018, **9**, 2905–2912.
17 V. R. Feig, H. Tran, M. Lee, K. Liu, Z. Huang, L. Beker, D. G. Mackanic and Z. Bao, *Adv. Mater.*, 2019, **31**, 1902869.
18 R. Ambrožič, U. Krühne and I. Plazl, *Chem. Eng. J.*, 2024, **485**, 149542.
19 X.-Z. Zhang, D.-Q. Wu and C.-C. Chu, *Biomaterials*, 2004, **25**, 3793–3805.
20 Y.-L. Zhao and J. F. Stoddart, *Langmuir*, 2009, **25**, 8442–8446.
21 D. Suhag, R. Bhatia, S. Das, A. Shakeel, A. Ghosh, A. Singh, O. P. Sinha, S. Chakrabarti and M. Mukherjee, *RSC Adv.*, 2015, **5**, 53963–53972.
22 Y. Xia, J. Guan and X. Du, *J. Energy Storage*, 2023, **72**, 108776.
23 J. Lin and X. Du, *Chem. Eng. J.*, 2022, **446**, 137244.
24 J. Wu, L. Wang, H. Yu, Z. Zain-ul-Abdin, R. U. Khan and M. Haroon, *J. Organomet. Chem.*, 2017, **828**, 38–51.
25 K. Kulbaba, M. J. MacLachlan, C. E. B. Evans and I. Manners, *Macromol. Chem. Phys.*, 2001, **202**, 1768–1775.
26 M. Ni, N. Zhang, W. Xia, X. Wu, C. Yao, X. Liu, X.-Y. Hu, C. Lin and L. Wang, *J. Am. Chem. Soc.*, 2016, **138**, 6643–6649.
27 Y. Habibi, L. A. Lucia and O. J. Rojas, *Chem. Rev.*, 2010, **110**, 3479–3500.
28 Z. Chen, Y. Hu, G. Shi, H. Zhuo, M. A. Ali, E. Jamróz, H. Zhang, L. Zhong and X. Peng, *Adv. Funct. Mater.*, 2023, **33**, 2214245.
29 S. R. S. Veloso, A. G. Azevedo, P. F. Teixeira and C. B. P. Fernandes, *Gels*, 2023, **9**, 574.
30 X. He and Q. Lu, *Carbohydr. Polym.*, 2023, **301**, 120351.
31 H. Xue, C. Zhu, Y. Wang, Q. Gu, Y. Shao, A. Jin, X. Zhang, L. Lei and Y. Li, *Mater. Today Bio*, 2025, **32**, 101814.
32 A. E. Way, L. Hsu, K. Shanmuganathan, C. Weder and S. J. Rowan, *ACS Macro Lett.*, 2012, **1**, 1001–1006.
33 S. Shafiei-Sabet, W. Y. Hamad and S. G. Hatzikiriakos, *Cellulose*, 2014, **21**, 3347–3359.
34 M. Chau, S. E. Sriskandha, D. Pichugin, H. Thérien-Aubin, D. Nykypanchuk, G. Chauve, M. Méthot, J. Bouchard, O. Gang and E. Kumacheva, *Biomacromolecules*, 2015, **16**, 2455–2462.
35 R. Prathapan, R. Thapa, G. Garnier and R. F. Tabor, *Colloids Surf., A*, 2016, **509**, 11–18.
36 S. Lombardo, A. Gençer, C. Schütz, J. Van Rie, S. Eyley and W. Thielemans, *Biomacromolecules*, 2019, **20**, 3181–3190.
37 K. H. M. Kan, J. Li, K. Wijesekera and E. D. Cranston, *Biomacromolecules*, 2013, **14**, 3130–3139.
38 D. M. Nascimento, Y. L. Nunes, M. C. B. Figueirêdo, H. M. C. De Azeredo, F. A. Aouada, J. P. A. Feitosa, M. F. Rosa and A. Dufresne, *Green Chem.*, 2018, **20**, 2428–2448.
39 R. Nasseri, C. P. Deutschman, L. Han, M. A. Pope and K. C. Tam, *Mater. Today Adv.*, 2020, **5**, 100055.
40 C. Hörenz, K. Bertula, T. Tiainen, S. Hietala, V. Hynninen and O. Ikkala, *Biomacromolecules*, 2020, **21**, 830–838.
41 R. Nasseri and K. C. Tam, *Mater. Adv.*, 2020, **1**, 1631–1643.
42 R. Nasseri, N. Bouzari, J. Huang, H. Golzar, S. Jankhani, X. Tang, T. H. Mekonnen, A. Aghakhani and H. Shahsavan, *Nat. Commun.*, 2023, **14**, 6108.
43 Y. Yang, H. Sun, M. Wang, M. Li, Z. Zhang, T. P. Russell and S. Shi, *Angew. Chem., Int. Ed.*, 2023, **62**, e202218440.
44 S. Eyley, S. Shariki, S. E. C. Dale, S. Bending, F. Marken and W. Thielemans, *Langmuir*, 2012, **28**, 6514–6519.
45 A.-L. Oechsle, L. Lewis, W. Y. Hamad, S. G. Hatzikiriakos and M. J. MacLachlan, *Chem. Mater.*, 2018, **30**, 376–385.
46 L. Lewis, PhD thesis, University of British Columbia, 2019, DOI: **10.14288/1.0380864**.
47 S. M. Puranik, A. C. Kumbharkhane and S. C. Mehrotra, *J. Chem. Soc., Faraday Trans.*, 1992, **88**, 433–435.
48 Q. Xu, F. Bu, C. Sun, X. Huang and H. Luo, *Carbohydr. Polym.*, 2023, **312**, 120830.
49 A. Harada, *Acc. Chem. Res.*, 2001, **34**, 456–464.

50 Y. Li, Z. Xu, Y. Liu, S. Jin, E. M. Fell, B. Wang, R. G. Gordon, M. J. Aziz, Z. Yang and T. Xu, *ChemSusChem*, 2021, **14**, 745–752.
51 S. Lu, T. Ma, X. Hu, Y. Zhou, T. Wang and Y. Song, *Int. J. Biol. Macromol.*, 2023, **225**, 198–206.
52 S.-T. Fei, M. V. B. Phelps, Y. Wang, E. Barrett, F. Gandhi and H. R. Allcock, *Soft Matter*, 2006, **2**, 397–401.
53 F. M. Fomin and K. S. Zaitseva, *Russ. J. Phys. Chem. A*, 2014, **88**, 466–470.

